AIAA Paper 2001-2606

GRID CONVERGENCE ERROR ANALYSIS FOR MIXED-ORDER NUMERICAL SCHEMES

Christopher J. Roy†

Sandia National Laboratories*

P. O. Box 5800, MS 0825

Albuquerque, NM 87185-0825

Abstract

New developments are presented in the area of grid convergence error analysis and error estimation for mixed-order numerical schemes. A mixed-order scheme is defined here as a numerical method where the order of the local truncation error varies either spatially (e.g., at a shock wave) or for different terms in the governing equations (e.g., first-order convection with second-order diffusion). The case examined herein is the Mach 8 laminar flow of a perfect gas over a sphere-cone geometry. This flowfield contains a strong bow shock wave where the formally second-order numerical scheme is reduced to first order via a flux limiting procedure. The mixed-order error analysis method allows for non-monotone behavior in the solutions variables as the mesh is refined. Non-monotonicity in the local solution variables is shown to arise from a cancellation of first- and second-order error terms for the present case. The proposed error estimator, which is based on the mixed-order analysis, is shown to provide good estimates of the actual error. Furthermore, this error estimator nearly always provides conservative error estimates, in the sense that the actual error is less than the error estimate, for the case examined.

Nomenclature

C_D	drag coefficient
C_f	skin friction coefficient
DE	discretization error
F_s	factor of safety *(F_s = 3)*
f	solution variable
g_i	i^{th} order error term coefficient
h	measure of grid spacing ($h_k = [N_1/N_k]^{1/2}$)
N	number of mesh cells
p	spatial order of accuracy
q	dynamic pressure, N/m^2
R_N	nose radius (R_N = 0.00508 *m*)
St	Stanton number (dimensionless heat transfer)
r	grid refinement factor
u	axial velocity component, *m/s*
x	axial coordinate, *m*
y	radial coordinate, *m*
$\varepsilon_{k+1,k}$	difference between a solution variable on mesh k+1 and mesh k ($\varepsilon_{k+1,k} = f_{k+1} - f_k$)
γ	ratio of specific heats (γ = 1.4)
ρ	density, kg/m^3

Subscripts and Superscripts

exact	exact value
inf	freestream value
k	mesh level, (k = 1, 2, 3, etc., fine to coarse)
n	flowfield node index
~	estimated value to order h^{p+1}

Introduction

As computers become faster and algorithms become more efficient, computational fluid dynamics (CFD) has enormous potential to contribute to the design, analysis, and certification of engineering systems. However, simulation results are often regarded with skepticism by the engineering community as a whole. Judging by the results of numerous blind validation studies,[1-3] this lack of confidence in CFD is not surprising. To quote one author,[2] "the results of such exercises can be highly user-

† Senior Member of Technical Staff, E-mail: cjroy@sandia.gov, Member AIAA

* Sandia is a multiprogram laboratory operated by Sandia Corporation, a Lockheed Martin Company, for the United States Department of Energy under Contract DE-AC04-94AL85000.

dependent even when the same CFD software with the same models is being used." Oftentimes, when a number of users do obtain the same results, these results do not agree with the experimental data. In order for CFD to achieve its potential, more work must be done to quantify the uncertainty in simulation results.

The uncertainty, or error, of a given CFD simulation can be categorized into two distinct areas.[4,5] Verification deals purely with the mathematics of a chosen set of equations, and can be thought of as "solving the equations right." Validation, on the other hand, entails a comparison to experimental data (i.e., the real world) and is concerned with "solving the right equations." With regards to the sequence, verification must be performed first for quantitative validation comparisons to be meaningful. Topics that are included under the broad heading of verification include coding errors, incomplete iterative convergence error, truncation error, round-off error, far-field boundary error, and grid convergence (or discretization) error. This last source of error is related to the adequacy of the computational mesh employed and is the focus of the current paper.

For complex problems, the most reliable methods[4] for assessing the grid convergence errors in the solution to partial differential equations are *a posteriori* methods based on Richardson Extrapolation. Roache has proposed a Grid Convergence Index[6] (*GCI*) as a uniform method for reporting the results of grid refinement studies. As a minimum requirement for demonstrating solution accuracy, two grid solutions are used along with a knowledge of the nominal order of accuracy of the numerical scheme to produce an error estimate in the solution properties. However, this minimum requirement can be misleading when the "observed" order of accuracy differs from the nominal order of accuracy. In Ref. 6, Roache further promotes the idea of using an additional grid level (or levels) in order to verify the order of accuracy of the numerical method and insure that the solutions are in the asymptotic grid convergence range.

Error analysis methods for high-speed compressible flows can be complicated by the presence of shock discontinuities. The most common numerical methods used for high-speed flows are characteristic-based upwind methods. For steady flows, methods that are second order in space are often employed due to their favorable mixture of accuracy and numerical stability. In order to prevent non-physical oscillations, most upwind schemes employ limiters which reduce the spatial accuracy to first order through shock waves. In fact, Van Leer showed that the capturing of a discontinuity without oscillation required that the spatial accuracy of the scheme reduce to first order.[7] The presence of both second- and first-order spatial accuracy (at discontinuities) can greatly complicate grid convergence analyses.

Carpenter and Casper[8] conducted a careful study of the grid convergence behavior for a two-dimensional hypersonic blunt-body flow. Their study employed higher-order methods and omitted any flux limiting at the shock wave. While the numerical schemes they employed were nominally third and fourth order, they found that the spatial order of accuracy always reverted to first order on sufficiently refined meshes. Their findings indicate that even without the use of flux limiters to reduce the spatial order of accuracy at discontinuities, the information is passed through the shock wave in a first-order manner (at least in two dimensions and higher). Similar results have been observed by other authors.[9-11] For shock-containing flows, it is surmised that the local truncation error reduces to first order at the discontinuity, regardless of the use of flux limiters. Since the truncation error determines the order of the method, this spatial variation in the truncation error results in a mixed-order scheme.

In addition to flows with shock waves, there are many other examples of mixed-order numerical schemes. Leonard's QUICK scheme[12] employs a third-order accurate convective operator and standard second-order central differences for diffusion. Celik et al.[13,14] examined the subsonic, backward-facing step problem with a numerical scheme which used central differences for the diffusion terms, but was a mixture of first-order upwind and second-order central difference for the convective terms. A mixed-order behavior can also occur for cases where the transport properties undergo large, abrupt changes, such as at the interface between two porous media.[4]

Previous work by Roy et al.[11,15] verified the presence of both first- and second-order errors for a hypersonic blunt-body flow with a nominally second-order numerical scheme. It was shown that the use of a mixed-order numerical scheme resulted in non-monotonic convergence of some of the flow properties as the mesh was refined. This non-monotonic grid convergence behavior was found to occur when the first- and second-order error terms were of opposite sign, thus leading to error cancellation. Non-monotonic grid convergence has been observed by a number of other authors. For example, Celik and Karatekin[14] examined the flow over a backward facing step using the k-ε turbulence model with wall functions. These authors found significant non-monotonicity in both the velocity and turbulent kinetic energy profiles as the grid was refined.

The two main goals of the current paper are to explore in detail the behavior of a mixed first- and second-order numerical scheme as the grid is refined and to develop an error estimator which can be applied to such schemes. The test problem used is the Mach 8 laminar flow of a perfect gas ($\gamma = 1.4$) over a sphere-cone geom-

etry. The accuracy of the surface pressure solutions on several grid levels was presented in Ref. 11 and included a detailed model validation study. These same calculations are explored further in the current paper, with a focus on the analysis and estimation of grid convergence errors.

Computational Model

The computational fluid dynamics code used herein is SACCARA, the Sandia Advanced Code for Compressible Aerothermodynamics Research and Analysis. The SACCARA code was developed from a parallel distributed memory version[16-19] of the INCA code,[20] originally written by Amtec Engineering. For the present simulations, the SACCARA code is used to solve the Navier-Stokes equations for conservation of mass, momentum, and energy in axisymmetric form. The perfect gas assumption is made, and the flow is further assumed to be laminar. Further details of the flowfield models employed can be found in Ref. 11. The governing equations are discretized using a cell-centered finite-volume approach. The convective fluxes at the interface are calculated using the Steger-Warming[21] flux vector splitting scheme. Second-order reconstructions of the interface fluxes are obtained via MUSCL extrapolation. The viscous terms are discretized using central differences.

A flux limiter is employed which reduces to first order in regions of large second derivatives of pressure and temperature. This limiting is used to prevent oscillations in the flow properties at shock discontinuities. The use of flux limiting results in a mixture of first- and second-order accuracy in space. The implications of the mixed-order scheme on the convergence behavior of the method as the grid is refined will be discussed in detail.

The SACCARA code employs a massively parallel distributed memory architecture based on multi-block structured grids. The solver is a Lower-Upper Symmetric Gauss-Seidel scheme based on the works of Yoon et al.[22,23] and Peery and Imlay,[24] which provides for excellent scalability up to thousands of processors.[25] The simulations presented herein were run using a single 400 MHz processor of a Sun Enterprise 10000 shared-memory machine.

Flowfield Conditions

The conditions used in the current simulations are presented below in Table 1. These conditions correspond to those employed in the Joint Computational Experimental Aerodynamics Program (JCEAP) experiment conducted at Sandia National Laboratories by Oberkampf and Aeschliman. This experimental data set consists of both force and moment data[26] as well as high-quality surface pressure data.[27,28] Since the focus of this paper is on the numerical accuracy of the simulations, comparisons to experimental data are omitted. See Ref. 11 for an extensive model validation study. For plotting purposes, the spatial coordinates are normalized by the nose radius (R_N=0.00508 *m*).

Table 1 Test conditions for JCEAP experiments

Flow Parameter	Value
Freestream Mach Number	7.841
Stagnation Pressure	2.4724×10^6 N/m^2
Stagnation Temperature	632.8 *K*
Freestream Static Pressure	286.8 N/m^2
Freestream Static Temperature	47.7 *K*
Freestream Unit Reynolds Number	$6.88\times10^6/m$
Freestream Dynamic Pressure	1.2344×10^4 N/m^2
Wall Temperature	316.7 *K*

Iterative Convergence

Iterative convergence was assessed by monitoring the L_2 norms of the residuals for the momentum equations. Since the flowfield is two-dimensional/axisymmetric, laminar, and has no flow separation or chemical reactions, the residuals were reduced down to machine zero (approximately fourteen orders of magnitude), thus insuring convergence of the iterative algorithm.

Extrapolation Techniques

The following development is based on a series expansion[4] of discretization error on mesh level *k*

$$DE_k = f_k - f_{exact} \tag{1}$$

where f_k is a discrete solution value on mesh level *k* and f_{exact} is the exact solution. Eq. (1) may be applied on a point-by-point basis locally within the domain or to global quantities (such as lift and drag). For a uniform mesh, this series expansion may be written as

$$f_k = f_{exact} + g_1 h_k + g_2 h_k^2 + g_3 h_k^3 + O(h_k^4) \tag{2}$$

where g_i is the ith order error term coefficient and h_k is some measure of the grid spacing on mesh k. For a second-order scheme, the g_1 coefficient will be zero. The general procedure is to write Eq. (2) for a number of different mesh levels and solve for an approximation to f_{exact} and the error term coefficients. In certain cases, a general error term of order p will be employed, where both the coefficients and this "observed" order p may be solved for. Without loss of generality, the fine grid spacing is normalized to unity (i.e., h_1=1), and the grid refinement factor is defined as

$$r_{k,k+1} = h_{k+1} / h_k \tag{3}$$

Some of the required assumptions for using these extrapolation methods are that the solutions must be in the asymptotic grid convergence range, the solutions must be smooth, and the local error should be an indication of the global error. Some of the caveats for using these extrapolation methods are that they tend to magnify round-off and incomplete iterative convergence error, and that the extrapolated solution generally does not obey the same conservation laws which are obeyed by the original solutions.

Standard Richardson Extrapolation

In the early 1900's, Richardson[29,30] developed a method of extrapolating two discrete second-order solutions to yield a fourth-order accurate solution. The solutions were obtained on a fine grid with spacing h_1 and a coarse grid with spacing h_2, with h_2/h_1=2 (i.e., grid doubling/halving). The fourth-order accuracy of the extrapolated solution arose from the use of central differences, which contain only even powers in the expansion given in Eq. (2). Unless central differences are used exclusively, the odd terms should be included, thus for a second-order numerical scheme, the two discrete solutions may be generally written as

$$\begin{aligned} f_1 &= f_{exact} + g_2 h_1^2 + O(h_1^3) \\ f_2 &= f_{exact} + g_2 h_2^2 + O(h_2^3) \end{aligned}$$

By neglecting the terms of order h^3 and higher, the above system can be solved for approximations to f_{exact} and g_2 (the coefficient of the second order error term)

$$\tilde{g}_2 = \frac{f_2 - f_1}{3h_1^2} \tag{4}$$

$$\tilde{f}_{exact} = f_1 + \frac{f_1 - f_2}{3} \tag{5}$$

where the overtilde (~) denotes approximate values which neglect higher-order terms. Defining the difference in two successive grid levels as

$$\varepsilon_{21} = f_2 - f_1 \tag{6}$$

and taking h_1=1, Eqs. (4) and (5) reduce to

$$\begin{aligned} \tilde{g}_2 &= \frac{1}{3}\varepsilon_{21} \\ \tilde{f}_{exact} &= f_1 - \frac{1}{3}\varepsilon_{21} \end{aligned} \tag{7}$$

In general, the above relations for $\tilde{g}_2$ and $\tilde{f}_{exact}$ are third-order accurate, however they will be fourth-order accurate when central differences are used. The assumption that h_1=1 and that the odd error terms are present will be used for the remainder of this section.

Generalized Richardson Extrapolation

The above Richardson Extrapolation technique can be generalized to arbitrary grid refinement factor r and order p following Roache.[4] The series representation is written as

$$\begin{aligned} f_1 &= f_{exact} + g_p h_1^p + O(h_1^{p+1}) \\ f_2 &= f_{exact} + g_p h_2^p + O(h_2^{p+1}) \end{aligned}$$

Approximating the above equations by dropping the higher-order terms and then solving for the p^{th} order error coefficient g_p and the exact solution f_{exact} results in

$$\tilde{g}_p = \frac{\varepsilon_{21}}{r^p - 1} \tag{8}$$

$$\tilde{f}_{exact} = f_1 - \frac{\varepsilon_{21}}{r^p - 1} \tag{9}$$

where $r = r_{12}$ from Eq. (3). In this case, the order of the discretization p must be assumed *a priori* since only two solutions are used. The above estimates will in general be $(p+1)^{th}$ order accurate.

In addition to using the extrapolated values to estimate the errors in the discrete solutions, it is strongly recommended that the order of accuracy also be verified. This type of order verification requires three discrete solutions *which are monotonic* as the grid is refined. Recovery of the formal order of accuracy of the scheme further requires that the three grid solutions be in the asymptotic grid convergence range. The series representation is now expressed as

$$f_1 = f_{exact} + g_p h_1^p + O(h_1^{p+1}) \quad (10)$$

$$f_2 = f_{exact} + g_p h_2^p + O(h_2^{p+1}) \quad (11)$$

$$f_3 = f_{exact} + g_p h_3^p + O(h_3^{p+1}) \quad (12)$$

If the higher order terms are neglected, then the above equations can be solved for approximations to the order p, g_p, and f_{exact} to give

$$\frac{r_{12}^{\tilde{p}} - 1}{r_{12}^{\tilde{p}} r_{23}^{\tilde{p}} - 1} = \frac{\varepsilon_{21}}{\varepsilon_{21} + \varepsilon_{32}} \quad (13)$$

$$\tilde{g}_p = \frac{\varepsilon_{21}}{r_{12}^{\tilde{p}} - 1} \quad (14)$$

$$\tilde{f}_{exact} = f_1 - \frac{\varepsilon_{21}}{r_{12}^{\tilde{p}} - 1} \quad (15)$$

Notice that Eq. (13) is transcendental in $\tilde{p}$, and thus must be solved iteratively (see Ref. 4). For the case when $r_{12} = r_{23} = r$ (i.e., constant grid refinement factor), this equation reduces to

$$\tilde{p} = \frac{\ln(\varepsilon_{32}/\varepsilon_{21})}{\ln(r)} \quad (16)$$

This last equation was used by de Vahl Davis in Ref. 31 to solve for the "observed" order of accuracy for the natural convection in a square cavity.

When the three discrete solutions do not converge monotonically as the grid is refined, then $\varepsilon_{32}/\varepsilon_{21} < 0$ and Eq. (16) is therefore undefined. Celik and Karatekin[14] addressed the issue of non-monotone, or "oscillatory," grid convergence by inserting a negative sign in front of the g_p coefficient in Eq. (11) (the medium mesh). However, mathematical justification for such a procedure is not well-founded. This paper will present both an analysis method and an error estimation technique for dealing with non-monotone grid convergence.

Mixed 1st + 2nd Order Extrapolation

For the case when both first- and second-order error terms are included,[11,15] three discrete solutions are needed, where the series representation is written as

$$f_1 = f_{exact} + g_1 h_1 + g_2 h_1^2 + O(h_1^3)$$

$$f_2 = f_{exact} + g_1 h_2 + g_2 h_2^2 + O(h_2^3)$$

$$f_3 = f_{exact} + g_1 h_3 + g_2 h_3^2 + O(h_3^3)$$

The inclusion of more than one error term in the expansion is not a new concept. For example, see Ref. 32 for a discussion of Romberg interpolation as applied to the trapezoidal rule. For arbitrary mesh refinement, the above equations may be solved for approximations to g_1, g_2, and f_{exact} to yield

$$\tilde{g}_1 = \frac{\varepsilon_{32}(1 - r_{12}^2) + \varepsilon_{21} r_{12}^2 (r_{23}^2 - 1)}{r_{12}(r_{12} - 1)(r_{23} - 1)(r_{12} r_{23} - 1)}$$

$$\tilde{g}_2 = \frac{\varepsilon_{32}(r_{12} - 1) - \varepsilon_{21} r_{12}(r_{23} - 1)}{r_{12}(r_{12} - 1)(r_{23} - 1)(r_{12} r_{23} - 1)}$$

$$\tilde{f}_{exact} = f_1 + \frac{\varepsilon_{32}(r_{12} - 1) - \varepsilon_{21}(r_{12} r_{23}^2 - r_{12} - r_{23} - 1)}{(r_{12} - 1)(r_{23} - 1)(r_{12} r_{23} - 1)}$$

For example, if $h_1 = 1$, $h_2 = 1.5$, and $h_3 = 2$, then $r_{12} = 3/2$ and $r_{23} = 4/3$, and the above equations simply reduce to

$$\tilde{g}_1 = -5\varepsilon_{32} + 7\varepsilon_{21}$$

$$\tilde{g}_2 = 2\varepsilon_{32} - 2\varepsilon_{21}$$

$$\tilde{f}_{exact} = f_1 + 3\varepsilon_{32} - 5\varepsilon_{21}$$

For the case of constant grid refinement factor, the above equations simplify to

$$\tilde{g}_1 = \frac{r^2 \varepsilon_{21} - \varepsilon_{32}}{r(r-1)^2} \quad (17)$$

$$\tilde{g}_2 = \frac{\varepsilon_{32} - r\varepsilon_{21}}{r(r+1)(r-1)^2} \quad (18)$$

$$\tilde{f}_{exact} = f_1 + \frac{\varepsilon_{32} - (r^2 + r - 1)\varepsilon_{21}}{(r+1)(r-1)^2} \quad (19)$$

and for $r = 2$, these equations further reduce to

$$\tilde{g}_1 = -\frac{1}{2}\varepsilon_{32} + 2\varepsilon_{21}$$

$$\tilde{g}_2 = \frac{1}{6}\varepsilon_{32} - \frac{1}{3}\varepsilon_{21}$$

$$\tilde{f}_{exact} = f_1 + \frac{1}{3}\varepsilon_{32} - \frac{5}{3}\varepsilon_{21}$$

The above estimates are generally third-order accurate. A third-order error term could be easily included by simply adding another mesh level (see Appendix A).

Flowfield Grids

Solutions were obtained for two different families of meshes. The first mesh family contains six grid refinement levels, from Mesh 1 (480×480 cells) to Mesh 6 (15×15 cells), with each successive grid level found by eliminating every other grid line in the two spatial dimensions (i.e., grid halving). The second family of meshes was obtained in the following fashion. A second-order accurate interpolation procedure was applied to a 960×960 mesh (not shown), resulting in a 1920×1920 cell mesh. Every third point was retained from this mesh, resulting in a 640×640 cell mesh (Mesh 0.5). This mesh, although not used, is the baseline mesh for the second family of meshes (Meshes 1.5 through 6.5) which are determined by again eliminating every other grid line in both directions. The meshes used in this study are summarized below in Table 2.

Table 2 Flowfield meshes

Mesh Name	Mesh Family[a]	Mesh Cells	Grid Spacing, h[b]
Mesh 1	A	480×480	1
Mesh 1.5	B	320×320	1.5
Mesh 2	A	240×240	2
Mesh 2.5	B	160×160	3
Mesh 3	A	120×120	4
Mesh 3.5	B	80×80	6
Mesh 4	A	60×60	8
Mesh 4.5	B	40×40	12
Mesh 5	A	30×30	16
Mesh 5.5	B	20×20	24
Mesh 6	A	15×15	32
Mesh 6.5	B	10×10	48

[a]Family A has ($3\cdot5\cdot2^n$, n=0, 1,..., 5) cells in each direction, while Family B has ($2\cdot5\cdot2^n$, n=0, 1,..., 5) cells in each direction
[b]The grid spacing measure is normalized by the grid spacing on the finest mesh (e.g., Mesh 1 has h=1)

Grid Convergence Error Analysis

A contour plot of Mach number is presented in Fig. 1 along with the flowfield mesh. The 60×60 mesh is used for clarity. A strong shock wave occurs in the domain roughly halfway between the body and the outer boundary. Along the stagnation streamline ($y/R_N = 0$), the shock is normal to the y-axis and is effectively grid aligned. For the remainder of the domain, the shock is generally not aligned with the mesh. In addition, no effort was made to cluster the grid to the shock.

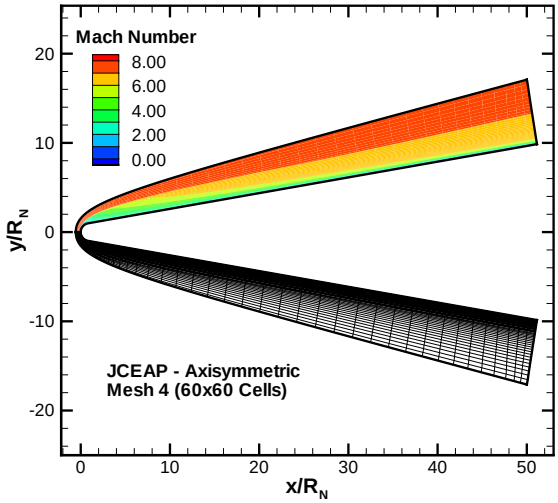

Fig. 1 Grid and Mach contours for JCEAP simulations.

The order of accuracy for the surface skin friction distributions has been calculated using Eq. (16) with $r = 2$ (see Fig. 2). Recall that the underlying assumption for this equation is that the solutions must change monotonically as the grid is refined. The results indicate that the local order of accuracy varies from negative values to values as large as nine. The undefined values, which are not included in the figure, occur when the argument of the natural logarithm in Eq. (16) is negative (i.e., the solutions are not monotonic). The failure of Eq. (16) to provide an "observed" order of accuracy close to the nominal order of the scheme (second order) provides the motivation for the current paper.

The first step towards quantifying the observed order of accuracy of the method is to examine the behavior of some norms of the spatial error. In order to calculate error norms, local estimates of the exact solution are required. Estimates of the exact solution were obtained by extrapolating the solutions using Meshes 1, 2, and 3 (restricted onto a 121×121 node mesh) using the 1st + 2nd order extrapolation method presented in Eqs. (17)-(19). Although not employed in the current work, Roache and Knupp[33] developed a method for obtaining estimates of

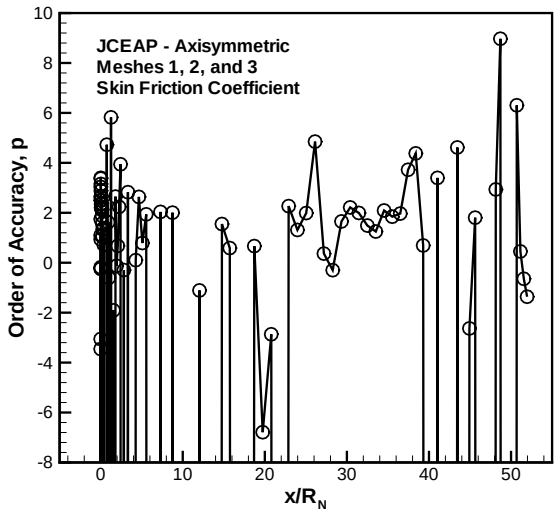

Fig. 2 Order of accuracy of the surface shear stress distributions from Eq. (16) using Meshes 1, 2, and 3.

the exact solution on the fine mesh points. The L_1 and L_2 norms were then calculated as follows:

$$L_1 \text{ norm}_k = \frac{\sum_{n=1}^{N} \left| f_{k,n} - \tilde{f}_{exact,n} \right|}{N}$$

$$L_2 \text{ norm}_k = \left(\frac{\sum_{n=1}^{N} \left| f_{k,n} - \tilde{f}_{exact,n} \right|^2}{N} \right)^{1/2}$$

where k indicates the mesh level and n is summed over the N points used in the norm calculation. Due to the requirement of three grids in the local calculation of $\tilde{f}_{exact}$ the norms for mesh Family A were calculated on either a 61×61 node mesh or the grid for Mesh k, whichever was smaller. For mesh Family B, the norms were calculated for the smaller of a 41×41 node mesh and the grid for Mesh k. All of the norms employed only half of the available flowfield points from the body out towards the shock. The omission of the shock wave was required since the extrapolation technique used to approximate f_{exact} is not valid for discontinuous solutions.

These norms are presented in Fig. 3 for the mass density and the axial component of velocity. The norms are all normalized to unity at the coarsest grid level (Mesh 6.5) for convenience. The norms are plotted versus the measure of the grid cell size h on a log-log plot. Recall that this cell size was normalized such that $h = 1$ on the finest mesh (Mesh 1). Since a grid refinement factor of two (grid halving) was used for each grid family, the discrete solutions for Family A fall at 1, 2, 4, 8, 16, and 32, and the discrete solutions for Family B fall at 1.5, 3, 6, 12, 24, and 48. The density norms exhibit nearly first-order behavior for all mesh sizes. The axial velocity exhibits a region of second-order behavior which asymptotes to a first-order slope on the finer meshes. The first-order asymptotic behavior as the mesh is refined is not unexpected, as discussed previously in the introduction.

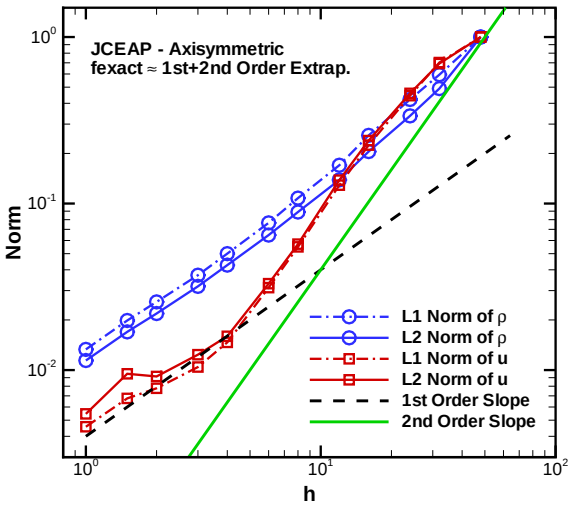

Fig. 3 Spatial error norms using half of the points from the body to the outer boundary (excluding the shock).

The general first-order convergence behavior for the flowfield density norms could be a result of either the first-order flux limiter at the shock wave or an error in the code. In the latter case, it is important to note that the code will produce the correct solutions based on prior validation work (see for example Ref. 11), but may approach these "correct solutions" at a less than second-order rate for certain flowfield properties. This reduction in order has been observed for relatively minor coding errors[34] (e.g., an incorrect array index, an incorrect constant in a difference operator, etc.).

The behavior of the surface heat transfer (Stanton number) with mesh refinement is presented in Fig. 4 at the axial location $x/R_N = 11.2$. For all but the coarsest mesh, the Stanton number converges monotonically as the grid is refined (i.e., as $h \to 0$). The solid line represents an estimate of the exact solution found from Eq. (19) using Meshes 1, 2, and 3. Further insight into the error behavior can be gained by examining the contributions of both the first- and second-order error terms.

Fig. 5 shows the behavior of the grid convergence error in the local Stanton number as the mesh is refined. The discrete solution error is calculated using the third-order accurate estimate for f_{exact} from Eq. (19) (using

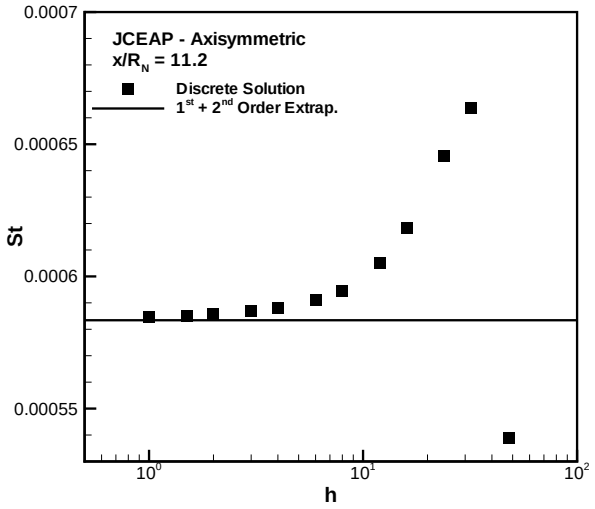

Fig. 4 Behavior of the Stanton number as the mesh is refined ($x/R_N = 11.2$).

Meshes 1, 2, and 3) and the following relationship:

$$|\text{Spatial Error (\%)}| = \left| \frac{f_k - \tilde{f}_{exact}}{\tilde{f}_{exact}} \right| \times 100 \qquad (20)$$

The discrete error appears as the square symbols in Fig. 5 and is expected to be a good representation of the true error, especially for the coarser meshes. Also shown in the figure are the normalized magnitudes of the first- and second-order error terms

$$\left| \frac{\tilde{g}_1 h}{\tilde{f}_{exact}} \right| \times 100 \quad \text{and} \quad \left| \frac{\tilde{g}_2 h^2}{\tilde{f}_{exact}} \right| \times 100 \qquad (21)$$

along with the magnitude of their sum:

$$\left| \frac{\tilde{g}_1 h + \tilde{g}_2 h^2}{\tilde{f}_{exact}} \right| \times 100 \qquad (22)$$

The first-order error term has a slope of unity on the log-log plot. For a first-order scheme, this first-order error term will dominate the second-order error term, and the discrete solution error will coincide with the first-order error. The second-order error term has a slope of two, and will dominate the total error when the scheme exhibiting second-order behavior. The magnitude of the sum of the two terms (solid line) is forced to pass through the points associated with Meshes 1, 2, and 3 since these solutions are used in the determination of the coefficients in Eqs. (17)-(19). First-order accuracy is seen in the fine grid solutions, while the error analysis predicts that the coarse grid solutions will begin to exhibit a second-order behavior. The grid convergence analysis, which uses only Meshes 1, 2, and 3, qualitatively predicts the reduction in error exhibited on the coarse meshes.

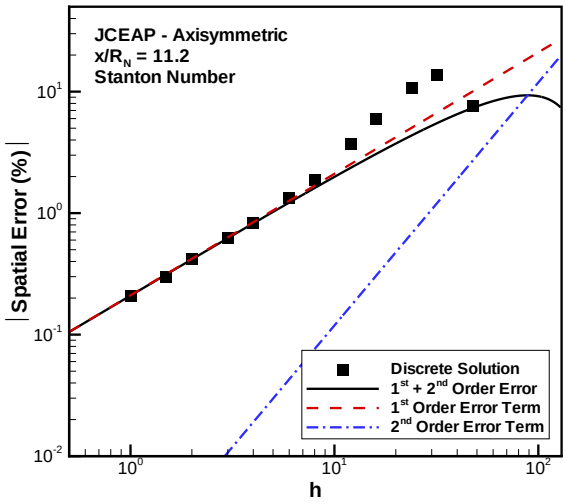

Fig. 5 Error in the Stanton number as the mesh is refined ($x/R_N = 11.2$).

The behavior of the skin friction coefficient as the mesh is refined is presented in Fig. 6 for the same axial location. In this case, the skin friction values first decrease as the grid is refined and then increase at $h = 1$. The spatial error in the skin friction as the grid is refined is presented in Fig. 7. The discrete skin friction values again exhibit a second-order behavior on the coarser meshes and a first-order behavior on the finer meshes. The coefficients of the first- and second-order error terms ($\tilde{g}_1$ and $\tilde{g}_2$) are of opposite sign, thus giving error cancellation when $\tilde{g}_1 h = -\tilde{g}_2 h^2$. This error cancellation manifests as a sharp drop in the error "predicted" from using Meshes 1, 2, and 3 (solid line). This error cancellation corresponds to the location where the discrete solutions cross over the estimated exact value in Fig. 6. As a result, the solution on Mesh 3 (120×120 cells) is actually estimated to have much less error than the finest mesh (Mesh 1 with 480×480 cells). The "predicted" error using Meshes 1, 2, and 3 (solid line) agrees well with the discrete solution errors shown in Fig. 7.

The estimated errors in the Stanton number at the stagnation point ($x/R_N = 0$) are given in Fig. 8. The error analysis again predicts error cancellation between the first- and second-order error terms. First-order behavior is evident for the fine mesh solutions, while coarser solutions also appear to have a second-order component. The agreement between the "predicted" error and the discrete error is not as good in this case.

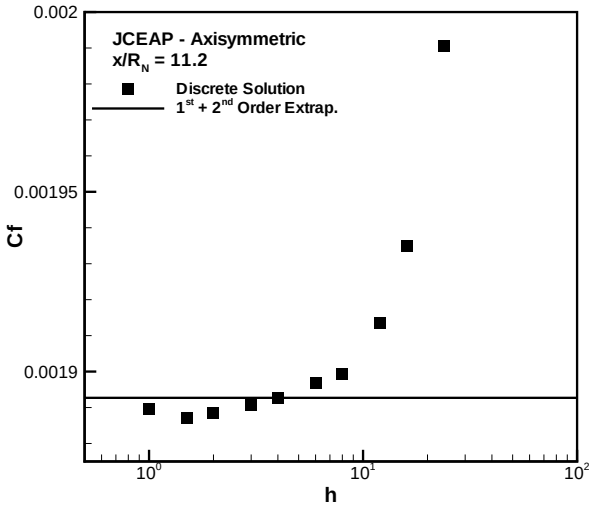

Fig. 6 Behavior of the skin friction coefficient as the mesh is refined ($x/R_N = 11.2$).

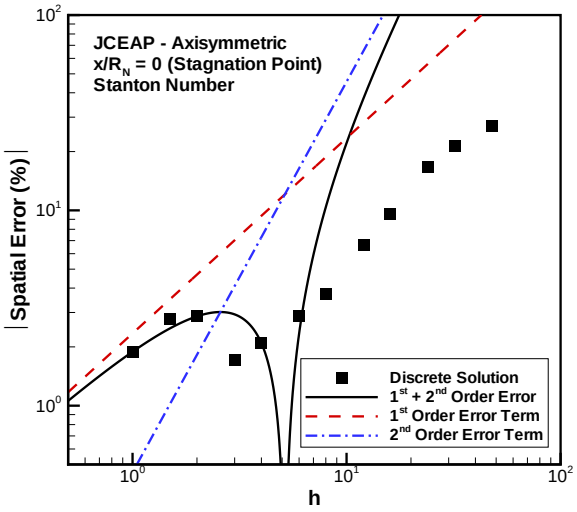

Fig. 8 Error in the Stanton number as the mesh is refined ($x/R_N = 0$).

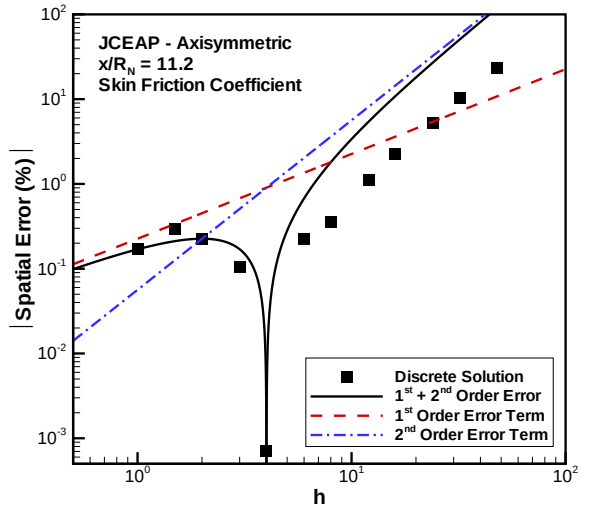

Fig. 7 Error in the skin friction coefficient as the mesh is refined ($x/R_N = 11.2$).

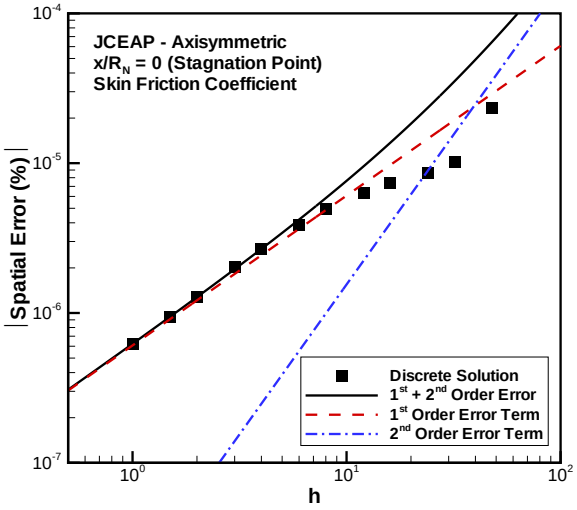

Fig. 9 Error in the skin friction coefficient as the mesh is refined ($x/R_N = 0$).

Error estimates for the skin friction at the stagnation point are shown in Fig. 9. Since the exact solution for the shear stress at the stagnation point is zero, the error terms in Eqs. (20)-(22) are normalized by the freestream dynamic pressure ($q_{inf} = 1.2344\times10^4$ N/m^2). The error analysis predicts that the error terms will be of the same sign and thus have a smooth transition from second order on the coarse meshes to first order as the mesh is refined. In this case, the first- and second-order coefficients ($\tilde{g}_1$ and $\tilde{g}_2$) have the same sign, so the magnitude of the sum of the error terms is larger than each of the individual error terms and the discrete solutions converge monotonically as the mesh is refined. The agreement between the "predicted" error and the discrete error is good for the finest meshes.

This error analysis has also been applied to the forebody drag, an integrated quantity. Fig. 10 gives the behavior of the drag coefficient as the mesh is refined. A non-monotone behavior is seen on the three coarsest meshes only. The spatial errors in the drag coefficient are presented in Fig. 11. Good agreement is again observed between the error analysis (using only Meshes 1, 2, and 3) and the discrete solution error for the finer meshes; however, the non-monotonic behavior on the three coarsest meshes is not captured in the error analysis.

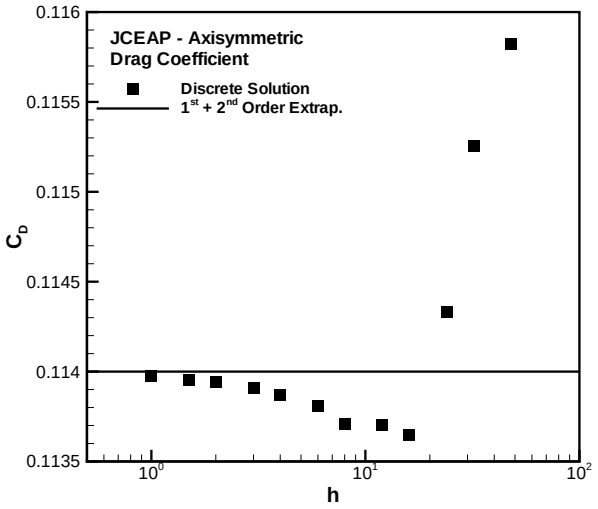

Fig. 10 Behavior of the forebody drag (excluding base drag) as the mesh is refined.

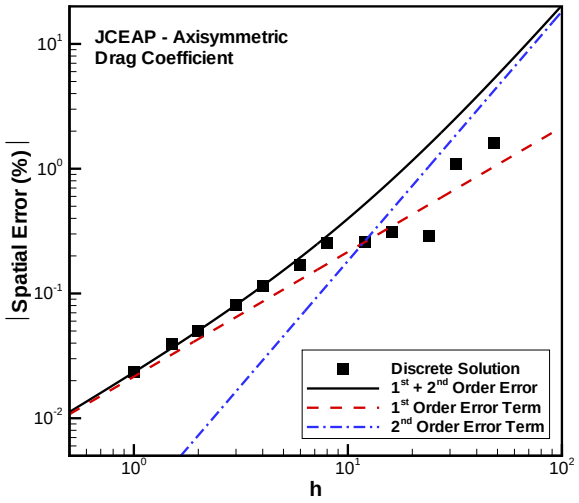

Fig. 11 Error in the forebody drag (excluding base drag) as the mesh is refined.

Grid Convergence Error Estimators

In the previous section, the focus was on error analysis and, specifically, on understanding how and why non-monotonic behavior can occur for flow properties as the mesh is refined. In this section, the focus now shifts to error estimation. The error estimation methods discussed below are intended to be used for engineering calculations where only a limited number of grid levels are available.

In Ref. 6, Roache encourages the use of at least three grid levels for problems sufficiently different than those previously studied. This position is also taken by the current author. If the three solutions converge monotonically as the mesh is refined, then the observed order of accuracy can be calculated with Eq. (16), and the generalized Richardson Extrapolation procedure of Eq. (15) can be employed using the two finest mesh levels. If the solutions do not converge monotonically, then the procedures developed in this section are recommended.

The goal of this section is to examine the behavior of a number of different error estimators for cases when the flowfield properties converge non-monotonically. The ideal error estimator would provide an error estimate that is very close to the actual error and carries some statistical measure of the confidence that the error estimate will be conservative (i.e., a 2σ or 95% confidence band). For complicated, nonlinear problems in multiple dimensions (and rarely in the true asymptotic grid convergence range), a rigorous proof of such an error band is probably not attainable.[4,6] We are therefore forced to rely on more heuristic methods of determining the uncertainties in CFD due to grid convergence errors.

The simplest method would be to simply use the extrapolated estimate of f_{exact} to estimate the error in the discrete solutions. For example, if the observed order of accuracy of some property has been verified (and the solutions are monotonic), then the generalized Richardson Extrapolation can be used to estimate the error from Eq. (20). However, since there is an equal possibility that the true exact solution is larger or smaller than the estimated f_{exact}, this method could be thought of as producing a 50% confidence band (i.e., there would be only a 50% chance that the true error estimate would be smaller than the estimated error). One approach would be to add a factor of safety to the error estimate of Eq. (20), such as

$$|\text{Spatial Error (\%)}| = F_s \left| \frac{f_k - \tilde{f}_{exact}}{\tilde{f}_{exact}} \right| \times 100 \qquad (23)$$

where the factor of safety can be chosen as some appropriate value (e.g., $F_s = 3$).

Another common approach to reporting grid convergence studies is to report the difference between a coarse grid solution f_2 and a fine grid solution f_1. These differences are generally reported as some percentage of the fine grid value. If the factor of safety is included, then this method could be expressed as

$$|\text{Spatial Error (\%)}| = F_s \left| \frac{f_2 - f_1}{f_1} \right| \times 100 \qquad (24)$$

In Ref. 6, Roache points out the main problems with this approach, namely that the error estimate is independent

of the order of accuracy of the numerical method or the grid refinement factor used. Clearly the true errors would be quite different if a 5% error is found using Eq. (24) for both a first-order scheme and a third-order scheme. A similar statement can be made for two cases where the grid refinement factor was $r = 2$ and $r = 1.1$. Roache has proposed a uniform method for reporting grid convergence studies which properly accounts for the order of accuracy of the method and the grid refinement factor.[6] Roache's Grid Convergence Index (*GCI*), on a percentage basis, is defined as

$$GCI(\%) = \frac{F_s}{r^p - 1}\left|\frac{f_2 - f_1}{f_1}\right| \times 100 \qquad (25)$$

where p is the order of the scheme, r is the grid refinement factor, and the factor of safety is generally taken to be $F_s = 3$. It can be shown that Eqs. (23) and (25) produce similar error estimates when the generalized Richardson Extrapolation method is used to determine $\tilde{f}_{exact}$ in Eq. (23) and when the *GCI* error estimate is less than 10-20% (see Appendix B for details). As presented in Eq. (25), the *GCI* is a fine grid error estimator. In Ref. 6, Roache presents a simple extension of the *GCI* to be used as a coarse grid error estimator. Coarse grid error estimates can be useful when a large number of parametric studies are required. In addition, all of these error estimators must be normalized by some reference value (other than $\tilde{f}_{exact}$) when $\tilde{f}_{exact}$ (or f_1 for the *GCI*) approaches zero.

Five different methods have been used to estimate the grid convergence errors. The first three methods all employ Eq. (23), but differ in that the estimate of the exact solution $\tilde{f}_{exact}$ is taken to be either the mixed $1^{st} + 2^{nd}$ order estimate of Eq. (19), or the generalized Richardson Extrapolation value of Eq. (9) with $p = 1$ or $p = 2$. Also shown in the figure is Roache's *GCI*(%) assuming either $p = 1$ or $p = 2$. The mixed $1^{st} + 2^{nd}$ order method required three solutions to obtain the estimate of the exact solution. Coarser meshes (from the same grid family) are used to provide the two additional solutions. For example, the $1^{st} + 2^{nd}$ order estimate at Mesh 4 will also use the discrete solutions on Meshes 5 and 6. The other estimators all require a single additional coarse grid, thus estimates are available on all but the coarsest meshes of each mesh family.

These estimates are compared to the best estimate error, which is determined using the mixed $1^{st} + 2^{nd}$ order extrapolation method on the three finest mesh solutions from grid Family A (Meshes 1, 2, and 3) and omitting the factor of safety (i.e., $F_s = 1$). This best estimate error is expected to be a very good error estimate, especially on the coarser meshes. These five error estimators are applied to the discrete values for the Stanton number at the $x/R_N = 11.2$ axial location for the various mesh levels, with the results shown in Fig. 12. For this case, all of the error estimation methods provide conservative estimates of the error over the entire range of grids. The differences between the first-order extrapolation of Eq. (23) and the first order *GCI*(%) are negligible until the estimates get as large as 10% ($h > 6$). It should be noted that the first-order *GCI* and the second-order *GCI* will, by definition, differ only by a factor of three (see Eq. (25)). The error estimator results for the skin friction at $x/R_N = 11.2$ are presented in Fig. 13. For this case, all of the error estimates are conservative with the exception of the second-order extrapolation (and second-order GCI) for $h = 1$ and $h = 2$. In addition, the mixed $1^{st} + 2^{nd}$ order extrapolation gives error estimates much closer to the actual (best estimate) error than the first-order methods.

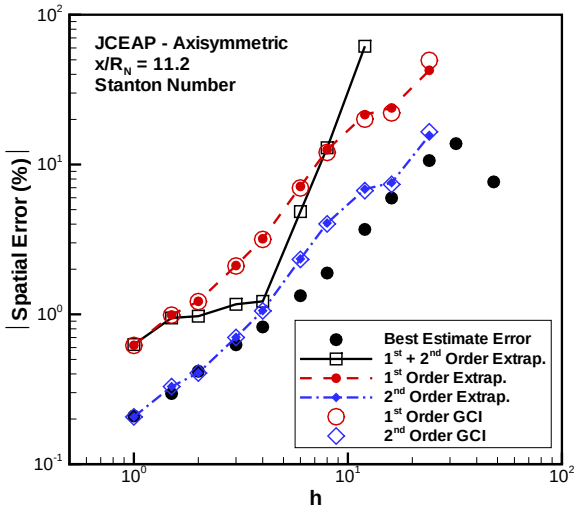

Fig. 12 Comparison of error estimates for the Stanton number ($x/R_N = 11.2$).

Error estimates for the Stanton number and the skin friction coefficient at the stagnation point are presented in Figs. 14 and 15, respectively. In both cases, the second-order error estimates fail to provide conservative error estimates on a significant number of the meshes. This figure highlights the dangers of simply employing the nominal order of the method (in this case second order) when the scheme is actually of mixed order. For the Stanton number, the mixed-order method provides conservative estimates of the error which are consistently better than the first-order estimates. For the skin friction coefficient, the first-order estimator and the mixed-order estimator give similar results except at h = 12, where the latter method is not conservative. It should be noted that this is the only location where the mixed-order error es-

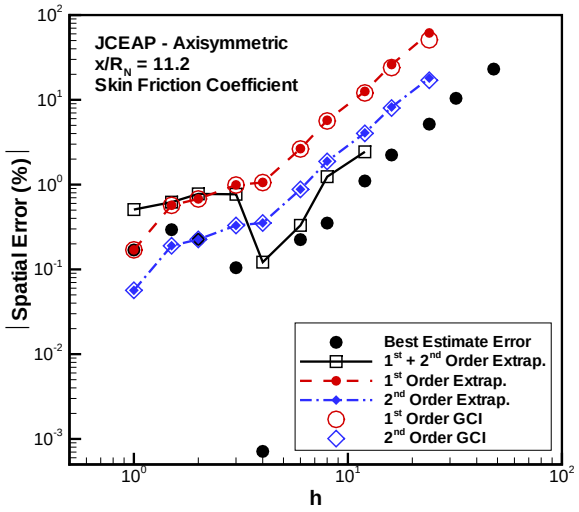

Fig. 13 Comparison of error estimates for the skin friction coefficient ($x/R_N = 11.2$).

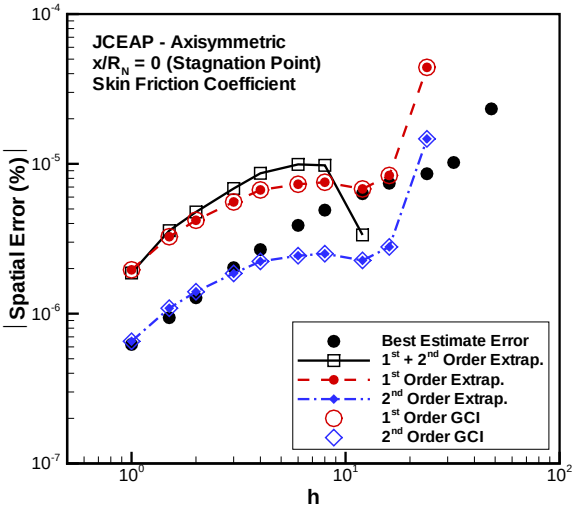

Fig. 15 Comparison of error estimates for the skin friction coefficient ($x/R_N = 0$).

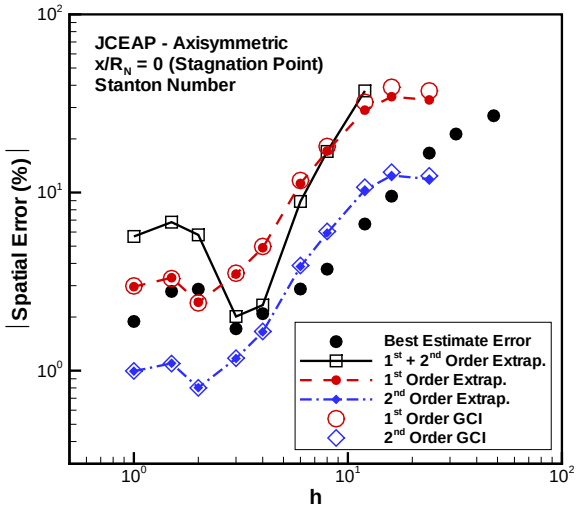

Fig. 14 Comparison of error estimates for the Stanton number ($x/R_N = 0$).

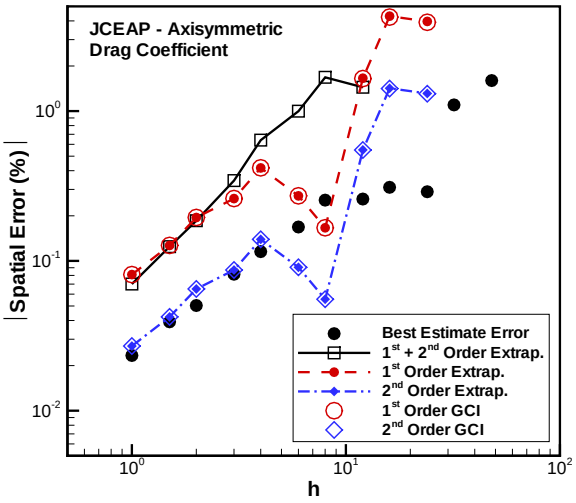

Fig. 16 Comparison of error estimates for the forebody drag (excluding base drag).

timator fails to provide a conservative estimate of the error for all cases examined in this paper.

Error estimates for the forebody drag coefficient are presented in Fig. 16. The mixed-order method is the only method that provides conservative error estimates on all mesh levels. The first-order estimates, while generally fairly good, do not give a conservative estimate of the error at $h = 8$.

Another possible error estimator is to determine an "observed" order of accuracy by a weighting of the first- and second-order error terms from the mixed-order method. These terms may be combined as

$$\tilde{p} = 1 + \frac{\left|\tilde{g}_2 h^2\right|}{\left|\tilde{g}_1 h\right| + \left|\tilde{g}_2 h^2\right|}$$

If a constant grid refinement factor is assumed as well as allowing $h = h_2$ for convenience, then the expressions for $\tilde{g}_1$ and $\tilde{g}_2$ from Eqs. (17) and (18) can be substituted into the above equation to produce

$$\tilde{p} = 1 + \frac{1}{\varphi + 1} \tag{26}$$

where

$$\varphi = \frac{r+1}{r}\left|\frac{\varepsilon_{32} - r^2\varepsilon_{21}}{\varepsilon_{32} - r\varepsilon_{21}}\right|$$

This "observed" order of accuracy can then be used with the generalized Richardson Extrapolation procedure to obtain an estimate of f_{exact} for use in Eq. (23). However, this method does not always produce conservative error estimates, as will be shown later. As an aside, this method for calculating the "observed" order of accuracy should be used with caution since it will always produce an order between one and two, regardless of the behavior of the discrete solutions. By no means can Eq. (26) be used to verify that a code is indeed providing second-order accurate solutions.

This p^{th} order extrapolation procedure has been applied to the drag coefficient results presented earlier and is shown in Fig. 17. The estimates appear to be similar to the first-order error estimates shown previously in Fig. 16, and are not conservative for $h = 8$. Also shown in the figure is the p^{th} order $GCI(\%)$ using the standard method for calculating the $\tilde{p}$ from Eq. (16). This method for calculating $\tilde{p}$ is undefined for $h = 4$, 6, and 8, and is thus not a useful error estimator for this problem. The p^{th} order error estimators have also been applied to the Stanton number at the stagnation point (see Fig. 18). The p^{th} order extrapolation fails the conservative test at $h = 1.5$ and 2, while the p^{th} order $GCI(\%)$ is undefined for $h < 3$.

Based on the above results, the best error estimation procedure for the current case is the mixed $1^{st} + 2^{nd}$ order method. This method almost always gave conservative estimates of the error, i.e., the error estimate was rarely smaller than the actual error. In addition, this method generally provided error estimates that were closer to the true (best estimate) error. The mixed $1^{st} + 2^{nd}$ order error estimator is therefore recommended for mixed-order problems. The first-order error estimator (along with the first-order GCI) also provided fairly good results, but failed to give conservative error estimates for certain cases where the solutions were not monotonic with grid refinement.

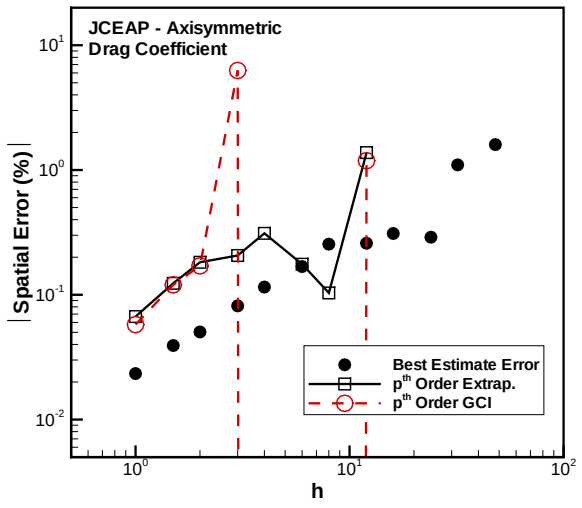

Fig. 17 Comparison of p^{th} order extrapolation error estimates for the forebody drag (excluding base drag).

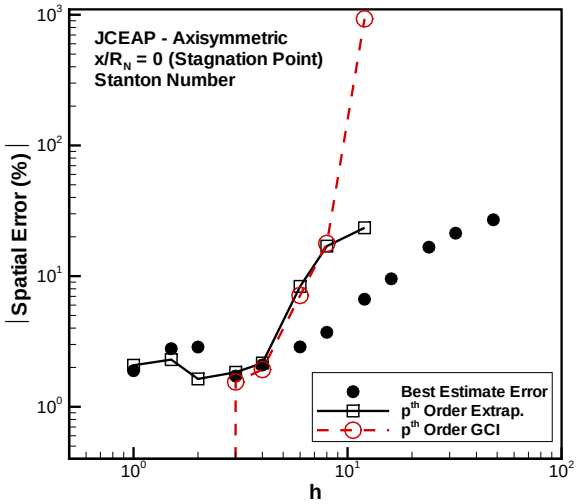

Fig. 18 Comparison of p^{th} order extrapolation error estimates for the Stanton number ($x/R_N = 0$).

The mixed $1^{st} + 2^{nd}$ order extrapolation has been applied to the surface and field properties of the current simulations using Mesh 1. The error estimates for the surface heat flux (Stanton number) and shear stress (skin friction coefficient) are presented in Fig. 19 and 20, respectively. The maximum errors in the heat flux occur at the stagnation point (6%) and at the sphere-cone tangency point (4%). With the exception of the stagnation region (where $C_f \to 0$ as $x/R_N \to 0$, thus requiring normalization of the error estimates) the maximum errors in the shear stress are approximately 3.5% and occur near the sphere-cone tangency point. The relatively large errors at the sphere-cone tangency point are due to the fact this point is a surface curvature discontinuity. Although not employed in this work, such singular points should be addressed either by additional grid refinement or other special treatment.

The field errors in the mass density are shown in Fig. 21 for the spherical nose region using Mesh 1. Although not shown, the errors were by far the largest at the shock wave, probably due to the poor estimate of the exact solution in the presence of the shock discontinuity (recall that the series expansion of Eq. (2) is not valid at

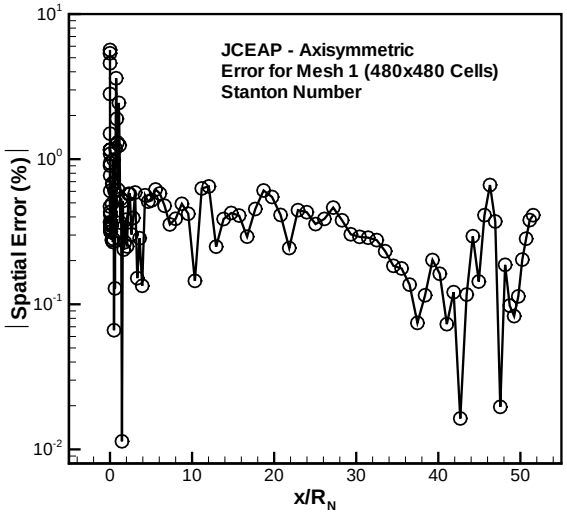

Fig. 19 Error estimates along the surface for the Stanton number.

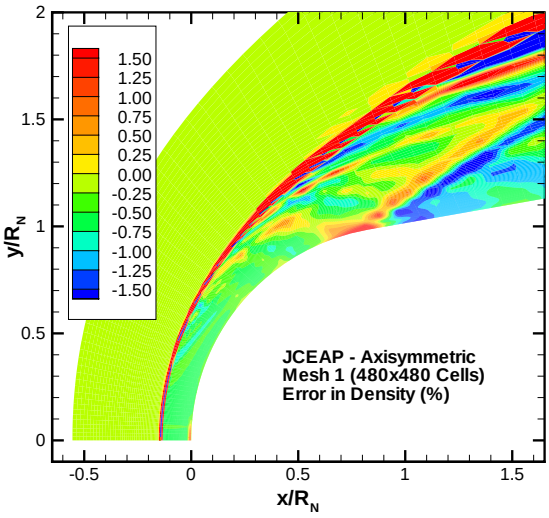

Fig. 21 Error estimates in the flowfield for the density.

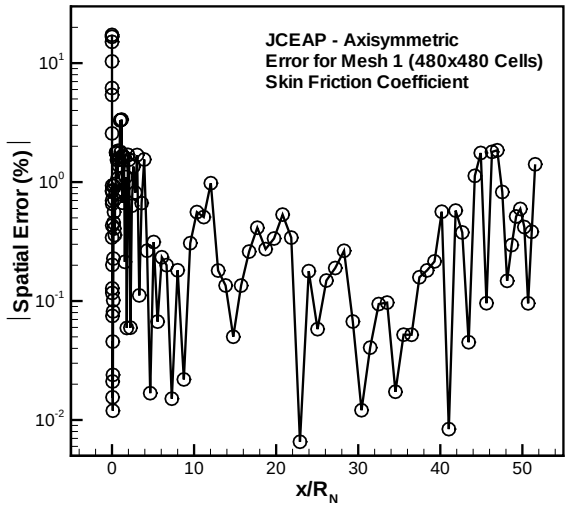

Fig. 20 Error estimates along the surface for the skin friction coefficient.

a discontinuity). The large errors at the shock wave are partly due the misalignment of the bow shock and the grid lines. Errors appear to convect downstream from the shock wave. The contour levels were scaled down to illustrate the behavior of the error between the shock and the body. Relatively large errors are also seen originating at the sphere-cone tangency point. Large errors at this location are expected since no effort was made to cluster the grid to this discontinuity in surface curvature (second derivative of surface position). The error appears to propagate from the sphere-cone tangency point along the characteristic Mach line.

Summary and Conclusions

Results were presented for the Mach 8 laminar flow of a perfect gas over a sphere-cone geometry. A formally second-order numerical method was employed; however, the spatial order of accuracy of the method was reduced to first order at the shock wave via a flux limiting procedure in order to prevent numerical oscillations. The numerical scheme is therefore mixed-order in the sense that the order of the local truncation error (which determines the order of accuracy of the scheme) varies from second order over most of the domain to first order at the shock wave. The first-order truncation error at the shock wave leads to the presence of a first-order discretization error component (however small) everywhere downstream. As the mesh spacing is refined, this first-order error component eventually dominates the total discretization error.

An error analysis method was presented for mixed-order numerical schemes in which both first- and second-order error terms were included. When the coefficients of these error components have the same sign, the convergence of the solution properties as the mesh is refined is monotone. However, when these coefficients are of opposite sign, error cancellation occurs at the crossover point where $\tilde{g}_1 h = -\tilde{g}_2 h^2$, resulting in non-monotonic behavior in the solution variables. The proposed mixed-order error analysis captures the non-monotone behavior of the solution variables, whereas methods based on linear extrapolation are unable to capture such features.

An error estimator was proposed which used a

mixed-order extrapolation to obtain an estimate of the exact solution. When combined with a factor of safety of three ($F_s = 3$), this mixed-order error estimator was shown to provide good local estimates of the error, even on fairly coarse meshes. This error estimator was further shown to provide conservative estimates of the error in almost all cases examined, in the sense that the true error was almost always smaller than the error estimate. Error estimators based on a locally "observed" order of accuracy were also examined, but were shown to fail for certain cases which exhibited non-monotonic solution behavior with grid refinement.

The error in the surface heat transfer (Stanton number) and surface shear stress (skin friction) was quantified using the mixed-order error estimator. The largest errors in the heat transfer were found to occur at the stagnation point (6%) and at the sphere-cone tangency point (4%). The largest errors in the surface shear stress were approximately 3.5% and occurred near the sphere-cone tangency point. A field plot of the mixed-order error estimated in the mass density also showed larger relative errors at the sphere-cone tangency point. These errors appear to propagate downstream along a characteristic Mach line. The sphere-cone tangency point is a surface curvature discontinuity and therefore requires grid clustering.

Further investigation into the grid convergence behavior of mixed-order numerical schemes is required. The nature of the local reduction to first order for flows with shock waves needs to be better understood. Examination of a "control" problem which does not contain shock waves would also be helpful. Finally, other sources of error which can influence the discretization error should be explored further including: mesh non-uniformities, boundary conditions, and singularities.

Appendices

Appendix A: Mixed 1st + 2nd + 3rd Order Extrap.

Although not employed in the current paper, it is possible to include first-, second-, and third-order error terms in the analysis. In this case, four grid levels must be used, and the series representation is

$$f_1 = f_{exact} + g_1 h_1 + g_2 h_1^2 + g_3 h_1^3 + O(h_1^4)$$
$$f_2 = f_{exact} + g_1 h_2 + g_2 h_2^2 + g_3 h_2^3 + O(h_2^4)$$
$$f_3 = f_{exact} + g_1 h_3 + g_2 h_3^2 + g_3 h_3^3 + O(h_3^4)$$
$$f_4 = f_{exact} + g_1 h_4 + g_2 h_4^2 + g_3 h_4^3 + O(h_4^4)$$

Neglecting terms of order h^4 and higher, the above set of equations can be solved for approximations to g_1, g_2, g_3, and f_{exact}. Assuming that the grid refinement factor is held constant, the above equations reduce to

$$\tilde{g}_1 = \frac{\varepsilon_{43} + r^2(\varepsilon_{21} r^3 - \varepsilon_{32}(r+1))}{r^2(r+1)(r-1)^3}$$
$$\tilde{g}_2 = \frac{-\varepsilon_{43} + r\varepsilon_{32}(r^2+1) - \varepsilon_{21} r^4}{r^3(r+1)(r-1)^3}$$
$$\tilde{g}_3 = \frac{\varepsilon_{43} - \varepsilon_{32} r(r+1) + \varepsilon_{21} r^3}{r^3(r+1)(r-1)^3(r^2+r+1)}$$
$$\tilde{f}_{exact} = f_1 + \frac{-\varepsilon_{43} + \varepsilon_{32}(r^3+r^2+r-1) - \varepsilon_{21}(r^5+r^4-r^2-r+1)}{(r+1)(r-1)^3(r^2+r+1)}$$

If the grid refinement factor is held constant at $r = 2$, then the above equations further reduce to

$$\tilde{g}_1 = \frac{1}{12}\varepsilon_{43} - \varepsilon_{32} + \frac{8}{3}\varepsilon_{21}$$
$$\tilde{g}_2 = -\frac{1}{24}\varepsilon_{43} + \frac{5}{12}\varepsilon_{32} - \frac{2}{3}\varepsilon_{21}$$
$$\tilde{g}_3 = \frac{1}{168}\varepsilon_{43} - \frac{1}{28}\varepsilon_{32} + \frac{1}{21}\varepsilon_{21}$$
$$\tilde{f}_{exact} = f_1 - \frac{1}{21}\varepsilon_{43} + \frac{13}{21}\varepsilon_{32} - \frac{43}{21}\varepsilon_{21}$$

The above equations are generally fourth-order accurate. Results for arbitrary grid refinement, although straightforward, are somewhat cumbersome and thus are omitted from the present work.

Appendix B: Relation Between Error Estimators

When the generalized Richardson Extrapolation method is used to estimate the exact solution f_{exact}, then the resulting error estimates, when combined with a factor of safety as in Eq. (23), can be shown to be approximately equivalent to Roache's Grid Convergence Index (*GCI*). Omitting the (×100) factor for simplicity, the definition for the error of Eq. (23) for the fine grid may be written as

$$|\text{Spatial Error}| = F_s \left| \frac{f_1 - \tilde{f}_{exact}}{\tilde{f}_{exact}} \right| \qquad \text{(A.1)}$$

Also recall the generalized Richardson extrapolation formula from Eq. (9)

$$\tilde{f}_{exact} = f_1 - \frac{f_2 - f_1}{r^p - 1} \qquad \text{(A.2)}$$

Substituting Eq. (A.2) into Eq. (A.1), and requiring that $r > 1$ and $p > 0$, results in

$$|\text{Spatial Error}| = F_s \left| \frac{\frac{f_2 - f_1}{r^p - 1}}{\tilde{f}_{exact}} \right| = \frac{F_s}{r^p - 1} \left| \frac{f_2 - f_1}{f_1} \right| \left| \frac{f_1}{\tilde{f}_{exact}} \right|$$

The first two terms on the right hand side are the *GCI*, thus we may write

$$|\text{Spatial Error}| \left| \frac{\tilde{f}_{exact}}{f_1} \right| = GCI$$

Taking the spatial error estimate (which uses the extrapolated value) as the more accurate estimate, we can calculate the error in the *GCI* as

$$\frac{GCI - |\text{Spatial Error}|}{|\text{Spatial Error}|} = \frac{\left| \frac{\tilde{f}_{exact}}{f_1} \right| - 1}{1}$$

Substituting Eq. (A.2) into the above relation yields

$$\frac{GCI - |\text{Spatial Error}|}{|\text{Spatial Error}|} = \left| \frac{f_1 - \frac{f_2 - f_1}{r^p - 1}}{f_1} \right| - 1 = |1 - \Phi| - 1$$

where

$$\Phi = \frac{1}{(r^p - 1)} \frac{f_2 - f_1}{f_1}$$

Notice that $|\Phi|$ is simply the *GCI* without the factor of safety F_s. Thus we can write

$$|\Phi| = \frac{GCI}{F_s}$$

So, when the $GCI < 300\%$, $|\Phi| < 1$, and we have

$$-1 < \Phi < 1, \quad \text{therefore} \quad |1 - \Phi| = 1 - \Phi$$

The error in the *GCI*, relative to Eq. (A.1) thus becomes

$$\frac{GCI - |\text{Spatial Error}|}{|\text{Spatial Error}|} = -\Phi$$

or, taking the absolute value

$$\left| \frac{GCI - |\text{Spatial Error}|}{|\text{Spatial Error}|} \right| = |\Phi| = \frac{GCI}{F_s} \qquad \text{(A.3)}$$

So the two error estimators are essentially equal when the Grid Convergence Index is small. These results are best summarized in Table A.1 below, where the two cases of $\Phi > 0$ and $\Phi < 0$ occur when the discrete solutions approach the exact solution from above and below, respectively. It is clear that for $GCI < 20\%$, these two error estimators provide similar results.

Table A.1 Differences in Error Estimators

GCI	|Spatial Error| ($\Phi < 0$)	|Spatial Error| ($\Phi > 0$)
3%	2.97%	3.03%
9%	8.73%	9.27%
15%	14.25%	15.75%
18%	16.92%	19.08%
21%	19.53%	22.47%

Acknowledgments

A number of people made valuable contributions to this paper. I would like to thank Fred Blottner and Bill Oberkampf of Sandia National Laboratories for their numerous discussions on grid convergence and error analysis. Thanks also go to Matt Hopkins of Sandia National Laboratories for his helpful discussions on numerical analysis and applied mathematics. Finally, I wish to thank Pat Roache of Ecodynamics Research Associates, Inc., who provided an extremely insightful review of many of the ideas presented herein. This work was supported by Sandia National Laboratories and the Department of Energy's Accelerated Strategic Computing Initiative.

References

1. "Best Practice Guidelines," ERCOFTAC Special Interest Group on Quality and Trust in Industrial CFD, M. Casey and T. Wintergerste, Eds., Jan. 2000.

2. Hutton, A. G., and Casey, M. V., "Quality and Trust in Industrial CFD - A European Initiative," AIAA Paper 2001-0656, Jan. 2001.

3. Harvey, J. K., Holden, M. S., and Wadhams, T. P., "Code Validation Study of Laminar Shock/Boundary Layer and Shock/Shock Interactions in Hypersonic Flow Part B: Comparison with Navier-Stokes and DSMC Solutions," AIAA Paper 2001-1031, Jan. 2001.

4. Roache, P. J., *Verification and Validation in Computational Science and Engineering*, Hermosa Publishers, New Mexico, 1998.

5. *Guide for the Verification and Validation of Computational Fluid Dynamics Simulations*, AIAA G-077-1998, p. 3.

6. Roache, P. J., "Perspective: A Method for Uniform Reporting of Grid Refinement Studies," *ASME Journal of Fluids Engineering*, Vol. 116, Sept. 1994, pp. 405-413.

7. Van Leer, B., "Towards the Ultimate Conservative Difference Scheme. I. The Quest of Monotonicity," *Lecture Notes in Physics*, Vol. 18, Springer Verlag, Berlin, 1973, pp. 163-168.

8. Carpenter, M. H., and Casper, J. H., "Accuracy of Shock Capturing in Two Spatial Dimensions," *AIAA Journal*, Vol. 37, No. 9, 1999, pp. 1072-1079.

9. Efraimsson, G., and Kreiss, G., "A Remark on Numerical Errors Downstream of Slightly Viscous Shocks," *SIAM Journal of Numerical Analysis*, Vol. 36, No. 3, 1999, pp. 853-863.

10. Engquist, B., and Sjogreen, B., "The Convergence Rate of Finite Difference Schemes in the Presence of Shocks," *SIAM Journal of Numerical Analysis*, Vol. 35, 1998, pp. 2464-2485.

11. Roy, C. J., McWherter-Payne, M. A., and Oberkampf, W. L., "Verification and Validation for Laminar Hypersonic Flowfields," AIAA Paper 2000-2550, June 2000.

12. Leonard, B. P., "A Stable and Accurate Convective Modelling Procedure Based on Quadratic Upstream Interpolation," *Computational Methods in Applied Mechanical Engineering*, Vol. 19, 1979, pp. 59-98.

13. Celik, I., and Zhang, W-M., "Calculation of Numerical Uncertainty Using Richardson Extrapolation: Application to Some Simple Turbulent Flow Calculations," *ASME Journal of Fluids Engineering*, Vol. 117, Sept. 1995, pp. 439-445.

14. Celik, I., and Karatekin, O., "Numerical Experiments on Application of Richardson Extrapolation with Nonuniform Grids," *ASME Journal of Fluids Engineering*, Vol. 119, Sept. 1997, pp. 584-590.

15. Roy, C. J., McWherter-Payne, M. A., and Oberkampf, W. L., "Verification and Validation for Laminar Hypersonic Flowfields Part 1: Numerical Error Assessment," manuscript in preparation for submittal to the *AIAA Journal*.

16. Wong, C. C., Soetrisno, M., Blottner, F. G., Imlay, S. T., and Payne, J. L., "PINCA: A Scalable Parallel Program for Compressible Gas Dynamics with Nonequilibrium Chemistry," SAND 94-2436, Sandia National Laboratories, Albuquerque, NM, 1995.

17. Wong, C. C., Blottner, F. G., Payne, J. L., and Soetrisno, M., "Implementation of a Parallel Algorithm for Thermo-Chemical Nonequilibrium Flow Solutions," AIAA Paper 95-0152, Jan. 1995.

18. Hassan, B., Kuntz, D. W., and Potter, D. L., "Coupled Fluid/Thermal Prediction of Ablating Hypersonic Vehicles," AIAA Paper 98-0168, Jan. 1998.

19. Kuntz, D. W., Hassan, B., and Potter, D. L., "An Iterative Approach for Coupling Fluid/Thermal Predictions of Ablating Hypersonic Vehicles," AIAA Paper 99-3460, June-July 1999.

20. INCA User's Manual, Version 2.0, Amtec Engineering, Inc., Bellevue, WA, 1995.

21. Steger, J. L., and Warming, R. F., "Flux Vector Splitting of the Inviscid Gasdynamic Equations with Applications to Finite Difference Methods," *Journal of Computational Physics*, Vol. 40, 1981, pp. 263-293.

22. Yoon, S., and Jameson, A., "An LU-SSOR Scheme for the Euler and Navier-Stokes Equations," AIAA Paper 87-0600, Jan. 1988.

23. Yoon, S., and Kwak, D., "Artificial Dissipation Models for Hypersonic External Flow," AIAA Paper 88-3708, 1988.

24. Peery, K. M., and Imlay, S. T., "An Efficient Implicit Method for Solving Viscous Multi-Stream Nozzle/Afterbody Flow Fields," AIAA Paper 86-1380, June 1986.

25. Payne, J. L., and Hassan, B., "Massively Parallel Computational Fluid Dynamics Calculations for Aerodynamics and Aerothermodynamics Applications," Proceedings of the 1998 HPCCP/CAS Workshop, NASA/CP-1999-208757, Jan. 1999, pp. 111-116.

26. Oberkampf, W. L., and Aeschliman, D. P., "Joint Computational/Experimental Aerodynamics Research on a Hypersonic Vehicle, Part 1: Experimental Results," *AIAA Journal*, Vol. 9, No. 3, 1995, pp. 432-437.

27. Oberkampf, W. L., Aeschliman, D. P., Henfling, J. F., and Larson, D. E., "Surface Pressure Measurements for CFD Code Validation in Hypersonic Flow," AIAA Paper 95-2273, June 1995.

28. Oberkampf, W. L., Aeschliman, D. P., Henfling, J. F., Larson, D. E., and Payne, J. L., "Surface Pressure Measurements on a Hypersonic Vehicle," AIAA Paper 96-0669, Jan. 1996.

29. Richardson, L. F., "The Approximate Arithmetical Solution by Finite Differences of Physical Problems Involving Differential Equations with an Application to the Stresses in a Masonry Dam," *Transactions of the Royal Society of London*, Ser. A 210, 1908, pp. 307-357.

30. Richardson, L. F., "The Deferred Approach to the Limit," *Transaction of the Royal Society of London*, Ser. A 226, 1927, pp. 229-361.

31. de Vahl Davis, G., "Natural Convection of Air in a Square Cavity: A Bench Mark Numerical Solution," *International Journal for Numerical Methods in Fluids*, Vol. 3, No. 3, 1983, pp. 249-264.

32. Ralston, A., "Ch. 4. Numerical Differentiation, Numerical Quadrature, and Summation," *A First Course in Numerical Analysis*, McGraw-Hill, New York, 1965, pp. 118-124.

33. Roache, P. J., and Knupp, P. M., "Completed Richardson Extrapolation," *Communications in Numerical Methods in Engineering*, Vol. 9, 1993, pp. 365-374.

34. Salari, K., and Knupp, P., "Code Verification by the Method of Manufactured Solutions," SAND 2000-1444, Sandia National Laboratories, Albuquerque, NM, 2000.